

Photovoltaic effect in an electrically tunable van der Waals heterojunction

Marco M. Furchi¹, Andreas Pospischil¹, Florian Libisch², Joachim Burgdörfer², and Thomas Mueller^{1,*}

¹*Vienna University of Technology, Institute of Photonics, Gusshausstraße 27-29, 1040 Vienna, Austria*

²*Vienna University of Technology, Institute for Theoretical Physics, Wiedner Hauptstraße 8-10, 1040 Vienna, Austria*

Semiconductor heterostructures form the cornerstone of many electronic and optoelectronic devices, such as the double-heterostructure laser¹. Traditionally, they are fabricated using epitaxial growth techniques. Recently, heterostructures have also been obtained by vertical stacking of two-dimensional crystals, such as graphene² and related materials³. These layered designer materials are held together by van der Waals forces and contain atomically sharp interfaces⁴. Here, we report a type-II van der Waals heterojunction made of molybdenum disulfide and tungsten diselenide monolayers⁵⁻⁹. The junction is electrically tunable and under appropriate gate bias, an atomically thin diode is realized. Upon optical illumination, charge transfer occurs across the planar interface and the device exhibits a photovoltaic effect. Advances in large-scale production of two-dimensional crystals¹⁰⁻¹² could thus lead to a new photovoltaic solar technology.

* Email: thomas.mueller@tuwien.ac.at

The discovery of the photovoltaic effect in a silicon p-n junction¹³ heralded the era of photovoltaics. Although today's technology is still mainly based on silicon, a multitude of other materials have been investigated since then, with perovskite¹⁴ being one of the most recent additions. Lately, a new class of materials has emerged – two-dimensional (2D) atomic crystals^{2, 3}. These can be produced at low costs and on flexible substrates, making them potentially attractive candidates for solar energy conversion. Most solar cell designs comprise an interface (junction) between two adjoining materials, at which the separation of the photo-generated charge carriers occurs. Schottky and p-n junctions have been realized in atomically thin transition metal dichalcogenides and the capability of 2D crystals for photovoltaics has been demonstrated^{15–18}. However, the lateral arrangement of these devices does not allow for easy scalability, for which a vertical geometry would be preferable. Such vertical heterostructures can be obtained by stacking different 2D crystals on top of each other^{4, 19–21}. The van der Waals interaction between the layers then keeps the stack together. In this letter, we demonstrate that a heterojunction made of two different dichalcogenides exhibits a photovoltaic effect and can be employed for solar-energy conversion.

Our devices (see Figure 1a for a schematic drawing) were fabricated on an oxidized silicon wafer with 300-nm-thick SiO₂. They consist of molybdenum disulfide (MoS₂) and tungsten diselenide (WSe₂) monolayers that were mechanically exfoliated from bulk crystals and stacked on top of each other. The details of the flake exfoliation/transfer process are outlined in the Methods section. Both flakes were then contacted with e-beam lithographically defined Pd/Au (40/60 nm) electrodes. A voltage V_G , applied to the silicon substrate, controls the electrical characteristics of the

heterojunction device. We investigated devices with MoS₂/WSe₂ and WSe₂/MoS₂ layer orders, which both displayed qualitatively similar behavior. Figure 1b shows a microscope image of one of our devices. Short circuits, caused by chunks of bulk material that are inevitably transferred with the monolayer flake, were removed using a focused ion beam (FIB). After sample fabrication the devices were annealed for at least eight hours at 380 K in vacuum ($\sim 10^{-5}$ mbar) to remove resist residues and other surface contaminants.

Before we discuss the device operation, let us recall the electronic properties of the materials used. Figure 1c shows schematic energy band diagrams of MoS₂ (left) and WSe₂ (right), respectively. Both are direct semiconductors when thinned to monolayer thickness^{22–24}, with band gaps of⁷ $E_{GM} = 1.8$ eV and⁹ $E_{GW} = 1.6$ eV at the K - and K' -points. As their gaps approximately match the solar spectrum they are both suitable as optical absorbers in a photovoltaic cell. The electron affinity (the energy required to excite an electron from the bottom of the conduction band to vacuum) of MoS₂ is⁷ $\chi_M = 4.2$ eV. Values reported for monolayer WSe₂ vary, but are generally lower⁹ ($\chi_W = 3.5$ – 4.0 eV), owing to the smaller electronegativity of W compared to Mo.

When brought into contact, an atomically-sharp van der Waals heterojunction is formed that is pristine and without broken bonds. The center part of Figure 1c shows the band diagram of the heterojunction, where, for simplicity, we assume flat band alignment with the neighboring monolayer regions. The exact band lineup will not only be governed by the intrinsic properties of the materials but also by extrinsic that vary from sample to sample and are hence difficult to predict. For example, strong and unintended n-doping is typically observed in natural MoS₂; adsorbed molecules from the ambient will give rise to

additional doping. The proposed band diagram in Figure 1c can hence only provide a qualitative picture. Because of the large energetic offset of the MoS₂ and WSe₂ states, interlayer coupling is negligible and the heterostructure bands can be considered as a superposition of the monolayer bands²⁵. Consequently, the lowest energy electron states are spatially located in the MoS₂ layer and the highest energy hole states lie in the WSe₂, thus forming a type-II heterostructure.

In a first step after device fabrication we acquired electrical characteristics, where the silicon substrate served as a back gate electrode to adjust the doping in the device. Figure 2a shows the current map as a function of gate (V_G) and bias (V) voltages, recorded under biasing conditions as shown in Figure 1a. The electrical characteristics are different from those obtained in ordinary MoS₂ or WSe₂ field-effect transistors⁵⁻⁹, but can readily be understood by considering an electrical series connection of two such transistors²⁶. While the MoS₂-channel remains n-type over most of the observed gate voltage range and gets fully depleted only at $V_G < -71$ V, the WSe₂-channel switches from n-type ($V_G > -11$ V) to p-type ($V_G < -47$ V) due to its ambipolar behavior. In the range -47 V $< V_G < -11$ V the WSe₂-sheet becomes intrinsic and the current flow is suppressed. The less efficient gating of MoS₂ as compared to WSe₂ is mainly attributed to the existence of impurity states underneath the conduction band through which the Fermi level moves slowly²⁷. The electrical transport in the MoS₂ then occurs by carriers that are thermally activated from impurity states to the conduction band²⁸.

The V -dependence of the current is strikingly different in the two on-states. At $V_G > -11$ V, when MoS₂ and WSe₂ are both n-type, current can flow under both V -polarities. In the range -71 V $< V_G < -47$ V, however, the current-voltage (J - V) characteristic

exhibits a nonlinear response with current flow only under forward ($V > 0$) bias. J - V traces obtained under n-n ($V_G = +10$ V) and p-n ($V_G = -59$ V) configurations are shown in Figure 2b as dashed blue and solid red lines, respectively. While the J - V curve of the n-n junction shows symmetric (resistive) behavior, the p-n configuration displays diode-like current rectification with a forward/reverse current ratio of $\sim 10^2$. The electrical characteristic can hence be controlled by electrostatic doping of both materials (see also Supplementary Figure 1).

Better insight in the diode operation is gained by the band diagram inset in Figure 2b. Forward biasing the diode drives electrons (holes) in MoS₂ (WSe₂) to the heterojunction, where they may either (1) overcome the conduction (valence) band offset to be injected into the neighboring layer and drift to the opposite contact electrode, or (2) recombine so that a continuous current is maintained. At this point it also becomes clear why we have chosen Pd as a contact metal. Pd has a high-work function which allows for efficient hole injection into²⁹ WSe₂, but still serves as a good n-type contact to MoS₂ (due to Fermi level pinning³⁰).

Figure 3a shows J - V curves upon illumination with white light from a halogen lamp with incident optical power P_{opt} varied between 180 and 6400 W/m² (different device than in Figure 2). The emission spectrum of the lamp is provided as Supplementary Figure 2. In all measurements the device is operated in the p-n regime, with V_G fixed at -50 V. From the J - V traces it is obvious that the device shows a photovoltaic response, as the curves pass through the fourth quadrant, and electrical power P_{el} can be extracted (Figure 3b). The illumination dependence of the diode series resistance is attributed to photo-gating³¹ of the MoS₂ (see Supplementary Figure 3 for

more information). Our physical picture of the photoresponse is the following (see inset of Figure 3a): After optical excitation, the photo-generated carriers relax to the lowest energy electron and hole states. These are spatially separated, and thus charge transfer across the heterojunction occurs. The relaxed carriers then diffuse to the opposing contacts, resulting in a photocurrent. From a molecular perspective used to describe organic solar cells, our device can be regarded as a heterojunction cell, in which the MoS₂ conduction and WSe₂ valence bands act as LUMO and HOMO levels, respectively. However, in contrast to organic cells, no exciton transport by diffusion is required in our devices, because of electron-hole pair (exciton) generation right at the junction. A spatially resolved photocurrent map (see Supplementary Figure 4b) was recorded using a tightly focused laser spot to verify that the photoresponse indeed stems from the laterally extended heterojunction and is not produced at one of the metal-semiconductor contacts¹⁵.

In Figures 3c and d we present short-circuit current J_{SC} and open-circuit voltage V_{OC} as a function of illumination intensity. The open symbols show values extracted from Figure 3a. Similar data are obtained by illumination at 532 nm wavelength with a solid-state laser (green symbols). The discrepancy in efficiencies is mainly attributed to the wavelength dependence of the optical absorption. J_{SC} shows no indication of saturation over the measured range of optical powers, which extends to intensities one order of magnitude higher than the terrestrial solar intensity. V_{OC} scales linearly with $\ln(P_{opt})$, as expected from conventional p-n junction theory. The power conversion efficiency is defined as $\eta = P_{el,m}/P_{opt}$, where $P_{el,m}$ denotes the output at the maximum power point, and is shown in Figure 3e (blue triangles). The fill factor is calculated according to

$FF = P_{el,m}/(J_{SC}V_{OC})$ and is plotted in the same figure (red squares). An efficiency of $\eta \approx 0.2\%$ is obtained, which is comparable to values reported for³² WSe₂ (0.1–0.6 %) and³³ MoS₂ (1 %) bulk samples, and, more recently, for lateral WSe₂ monolayer p-n junctions^{16, 17} (0.2–0.5 %). The device can also be operated as a photodiode by biasing it in the third quadrant. At $V = -1$ V, a photoresponsivity of $R = 11$ mA/W is achieved. The external quantum efficiency, which is the ratio of the number of collected charge carriers to the number of incident photons, is $EQE = Rhc/(\lambda e) \approx 2.1\%$, where h , c , and e denote Planck's constant, speed of light, and electron charge, respectively, and $\lambda \approx 650$ nm is the wavelength. We note that these numbers need to be judged in the light of the weak optical absorption (5–10 %) of the ultra-thin 2D structure. A 10–20 fold increase may be achieved by stacking several junctions on top of each other, or by plasmonic enhancement of the optical absorption³⁴. Moreover, in our present proof-of-principle devices, photo-generated carriers can recombine during their lateral diffusion to the contacts. Better results could thus be obtained by sandwiching the dichalcogenide junction between two sheets of graphene or other transparent electrodes for vertical carrier extraction^{21, 35}.

In Figure 4 we show J_{SC} (red symbols) and V_{OC} (blue symbols) as a function of gate voltage (see corresponding $J-V$ curves in Supplementary Figure 5). The photocurrent clearly peaks in the p-n regime ($V_G = -50$ V), whereas it is suppressed for other gate voltages. The reason for this behavior is twofold. (1) A large gate-induced excess carrier concentration (electrons in MoS₂ for $V_G \gg -50$ V; holes in WSe₂ for $V_G \ll -50$ V) reduces the minority carrier lifetime and gives rise to enhanced recombination of the photo-generated carriers. The drop in open-circuit voltage to both sides of the p-n

regime provides evidence for this claim. (2) The carrier collection efficiency depends on V_G because of the gate-dependent band alignment along the channel of the device.

Given the rapid advances in large-scale production of 2D crystals¹⁰⁻¹², we see potential for using van der Waals heterojunctions in photovoltaic energy conversion. The ability of bringing together different 2D materials in a roll-to-roll process could lead to a new photovoltaic solar technology. Due to the plurality of different 2D materials, even low-cost multi-junction solar cells could come within reach.

Methods

Bulk crystals of MoS₂ and WSe₂ were purchased from *SPI Supplies* and *Nanosurf Inc.*, respectively, mechanically exfoliated, and then transferred to produce the heterojunction. In a first step, the bottom-layer flake was exfoliated directly onto the Si/SiO₂ substrate, identified by optical microscopy, and its thickness verified by Raman spectroscopy. In a second step, the top-layer flake was exfoliated onto a stack of polymers on a sacrificial silicon wafer. The polymer stack consisted of polyacrylic acid (PAA) and polymethyl methacrylate (PMMA), with a thickness chosen such that a monolayer flake could again be identified using a microscope. The PAA was then dissolved in water and the PMMA with the monolayer flake was released from the wafer, turned upside down, and placed with micrometer-precision on top of the other flake, with the target wafer kept at 380 K (above the glass transition temperature of PMMA). Finally, the wafer was cooled down to room temperature and the PMMA was dissolved.

Electrical measurements were performed in a wafer probe station using a semiconductor parameter analyzer (Agilent 4155C). The photovoltaic response was

measured with white light from a halogen lamp, that we focused with a microscope objective onto the sample. For details on the photocurrent imaging measurements see Supplementary Figure 4a.

Acknowledgements

We would like to thank Georg Kresse, Kerstin Hummer, and Karl Unterrainer for valuable discussions, Markus Schinnerl and Garrett D. Cole for technical assistance, and Emmerich Bertagnolli for providing access to a Raman spectrometer. The research leading to these results has received funding from the Austrian Science Fund FWF (START Y-539) and the European Union Seventh Framework Programme (grant agreement no. 604391 Graphene Flagship).

Author Contributions

T.M. conceived the experiment. M.F. fabricated the devices and carried out the measurements. A.P. contributed to the sample fabrication. M.F., F.L., J.B., and T.M. analyzed the data. T.M. prepared the manuscript. All authors discussed the results and commented on the manuscript.

References

1. Kroemer, H. A Proposed Class of Heterojunction Injection Lasers. *Proc. IEEE* **51**, 1782–1783 (1963).
2. Novoselov, K. S. *et al.* Electric field effect in atomically thin carbon films. *Science* **306**, 666–669 (2004).
3. Novoselov, K. S. *et al.* Two-dimensional atomic crystals. *Proc. Natl. Acad. Sci.* **102**, 10451–10453 (2005).
4. Geim, A. K. & Grigorieva, I. V. Van der Waals heterostructures. *Nature* **499**, 419–425 (2013).
5. Radisavljevic, B., Radenovic, A., Brivio, J., Giacometti, V. & Kis, A. Single-layer MoS₂ transistors. *Nat. Nanotechnol.* **6**, 147–150 (2011).
6. Podzorov, V., Gershenson, M. E., Kloc, Ch., Zeis, R. & Bucher, E. High-mobility field-effect transistors based on transition metal dichalcogenides. *Appl. Phys. Lett.* **84**, 3301–3303 (2004).
7. Wang, Q. H., Kalantar-Zadeh, K., Kis, A., Coleman, J. N. & Strano, M. S. Electronics and optoelectronics of two-dimensional transition metal dichalcogenides. *Nat. Nanotechnol.* **7**, 699–712 (2012).
8. Jariwala, D., Sangwan, V. K., Lauhon, L. J., Marks, T. J. & Hersam, M. C. Emerging Device Applications for Semiconducting Two-Dimensional Transition Metal Dichalcogenides. *ACS Nano* **8**, 1102–1120 (2014).
9. Liu, W., Kang, J., Sarkar, D., Khatami, Y., Jena, D. & Banerjee, K. Role of Metal Contacts in Designing High-Performance Monolayer n-Type WSe₂ Field Effect Transistors. *Nano Lett.* **13**, 1983–1990 (2013).
10. Bae, S. *et al.* Roll-to-roll production of 30-inch graphene films for transparent electrodes. *Nat. Nanotechnol.* **5**, 574–578 (2010).
11. Liu, K.-K. *et al.* Growth of Large-Area and Highly Crystalline MoS₂ Thin Layers on Insulating Substrates. *Nano Lett.* **12**, 1538–1544 (2013).
12. Huang, J.-K. *et al.* Large-Area Synthesis of Highly Crystalline WSe₂ Monolayers and Device Applications. *ACS Nano* **8**, 923–930 (2014).

13. Chapin, D. M., Fuller, C. S. & Pearson, G. L. A new silicon p-n junction photocell for converting solar radiation into electrical power. *J. Appl. Phys.* **25**, 676–677 (1954).
14. Lee, M. M., Teuscher, J., Miyasaka, T., Murakami, T. N. & Snaith, H. J. Efficient Hybrid Solar Cells Based on Meso-Superstructured Organometal Halide Perovskites. *Science* **338**, 643–647 (2012).
15. Fontana, M. *et al.* Electron-hole transport and photovoltaic effect in gated MoS₂ Schottky junctions. *Sci. Rep.* **3**, 1634 (2013).
16. Pospischil, A., Furchi, M. M. & Mueller, T. Solar-energy conversion and light emission in an atomic monolayer p-n diode. *Nat. Nanotechnol.* (in press).
17. Baugher, B. W. H., Churchill, H. O. H., Yafang, Y. & Jarillo-Herrero, P. Optoelectronics with electrically tunable PN diodes in a monolayer dichalcogenide. *Nat. Nanotechnol.* (in press).
18. Ross, J. S. *et al.* Electrically Tunable Excitonic Light Emitting Diodes based on Monolayer WSe₂ p-n Junctions. *Nat. Nanotechnol.* (in press).
19. Dean, C. *et al.* Graphene based heterostructures. *Solid State Comm.* **152**, 1275–1282 (2012).
20. Georgiou, T. *et al.* Vertical field-effect transistor based on graphene-WS₂ heterostructures for flexible and transparent electronics. *Nat. Nanotechnol.* **8**, 100–103 (2013).
21. Britnell, L. *et al.* Strong light-matter interactions in heterostructures of atomically thin films. *Sci. Express* **340**, 1311–1314 (2013).
22. Mak, K. F., Lee, C., Hone, J., Shan, J. & Heinz, T. F. Atomically thin MoS₂: a new direct-gap semiconductor. *Phys. Rev. Lett.* **105**, 115409 (2009).
23. Splendiani, A. *et al.* Emerging Photoluminescence in Monolayer MoS₂. *Nano Lett.* **10**, 1271–1275 (2010).
24. Tonndorf, P. *et al.* Photoluminescence emission and Raman response of monolayer MoS₂, MoSe₂, and WSe₂. *Opt. Express* **21**, 4908–4916 (2013).
25. Kośmider, K. & Fernández-Rossier, J. Electronic properties of the MoS₂-WS₂ heterojunction. *Phys. Rev. B* **87**, 075451 (2013).

26. Jariwala, D. *et al.* Gate-tunable carbon nanotube–MoS₂ heterojunction p-n diode. *Proc. Natl. Acad. Sci.* **110**, 18076–18080 (2013).
27. Ayari, A., Cobas, E., Ogundadegbe, O. & Fuhrer, M. S. Realization and electrical characterization of ultrathin crystals of layered transition-metal dichalcogenides. *J. Appl. Phys.* **101**, 014507 (2007).
28. Ghatak, S., Pal, A. N. & Ghosh, A. Nature of Electronic States in Atomically Thin MoS₂ Field-Effect Transistors. *ACS Nano* **5**, 7707–7712 (2011).
29. Fang, H. *et al.* High-Performance Single Layered WSe₂ p-FETs with Chemically Doped Contacts. *Nano Lett.* **12**, 3788–3792 (2012).
30. Das, S., Chen, H.-Y., Penumatcha, A. V. & Appenzeller, J. High Performance Multilayer MoS₂ Transistors with Scandium Contacts. *Nano Lett.* **13**, 100–105 (2013).
31. Lopez-Sanchez, O., Lembke, D., Kayci, M., Radenovic, A. & Kis, A. Ultrasensitive photodetectors based on monolayer MoS₂. *Nat. Nanotechnol.* **8**, 497–501 (2013).
32. Späh, R., Elrod, U., LuxSteiner, M., Bucher, E. & Wagner, S. pn junctions in tungsten diselenide. *Appl. Phys. Lett.* **43**, 79–81 (1983).
33. Fortin, E. & Sears, W. M. Photovoltaic effect and optical absorption in MoS₂. *J. Phys. Chem. Solids* **43**, 881–884 (1982).
34. Echtermeyer, T. J. *et al.* Strong plasmonic enhancement of photovoltage in graphene. *Nat. Commun.* **2**, 458 (2011).
35. Yu, W. J. *et al.* Highly efficient gate-tunable photocurrent generation in vertical heterostructures of layered materials. *Nat. Nanotechnol.* **8**, 952–958 (2013).

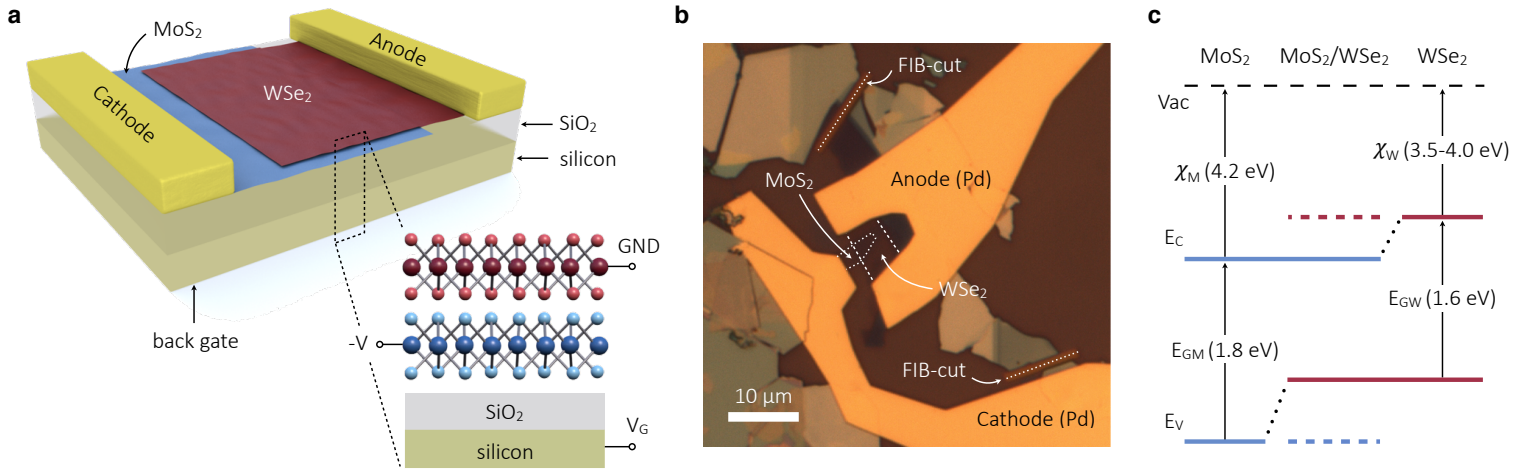


Figure 1. Van der Waals heterojunction device and band diagram. (a) Schematic drawing of the device structure. (b) Microscope image of a typical device. Contact electrodes are made of Pd/Au. The MoS₂ and WSe₂ monolayer flakes are highlighted by dotted and dashed lines, respectively. Short circuits are removed using a focused ion beam (dotted lines). (c) Schematic energy band diagrams of MoS₂ (left; blue lines) and WSe₂ (right; red lines) in the vicinity of the K-point. The MoS₂/WSe₂ heterostructure bands (center) are a superposition of the monolayer bands. The lowest energy electron states (solid blue line) are spatially located in the MoS₂ layer and the highest energy hole states (solid red line) lie in the WSe₂. The excited states are shown as dashed lines and do not play a role in device operation. E_C , conduction band edge; E_V , valence band edge; Vac , vacuum level.

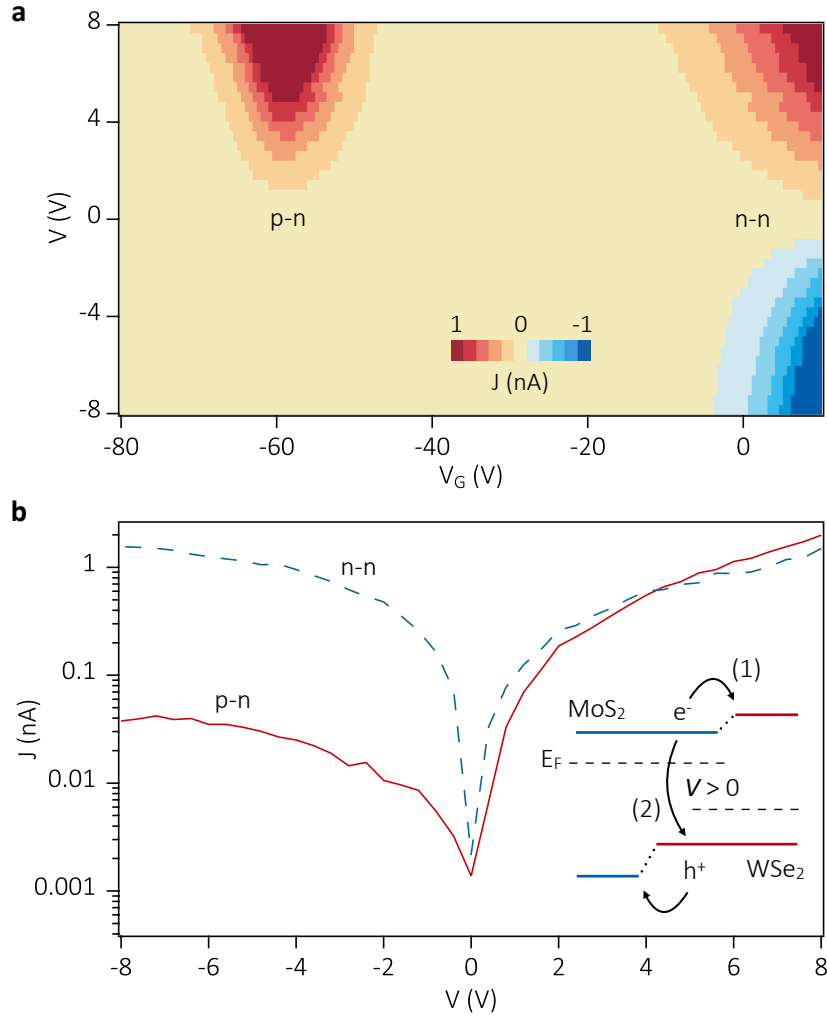


Figure 2. Electrical characteristic of the heterojunction. (a) Current map, recorded by scanning gate voltage V_G and bias voltage V . At $V_G > -10$ V, both flakes are n-type and the device shows resistive behavior. In the range -71 V $< V_G < -47$ V, the electrical characteristic exhibits a p-n diode-like behavior. (b) J - V traces obtained under n-n ($V_G = +10$ V; dashed blue line) and p-n ($V_G = -59$ V; solid red line) operation (absolute value of the device current J on a logarithmic scale). Inset: Band diagram under p-n operation and forward bias ($V > 0$). Electrons (e^-) and holes (h^+) are injected into the MoS₂ and WSe₂ sheets, respectively, and drift towards the junction where they may (i) overcome the band offsets, or (ii) recombine. E_F , Fermi level.

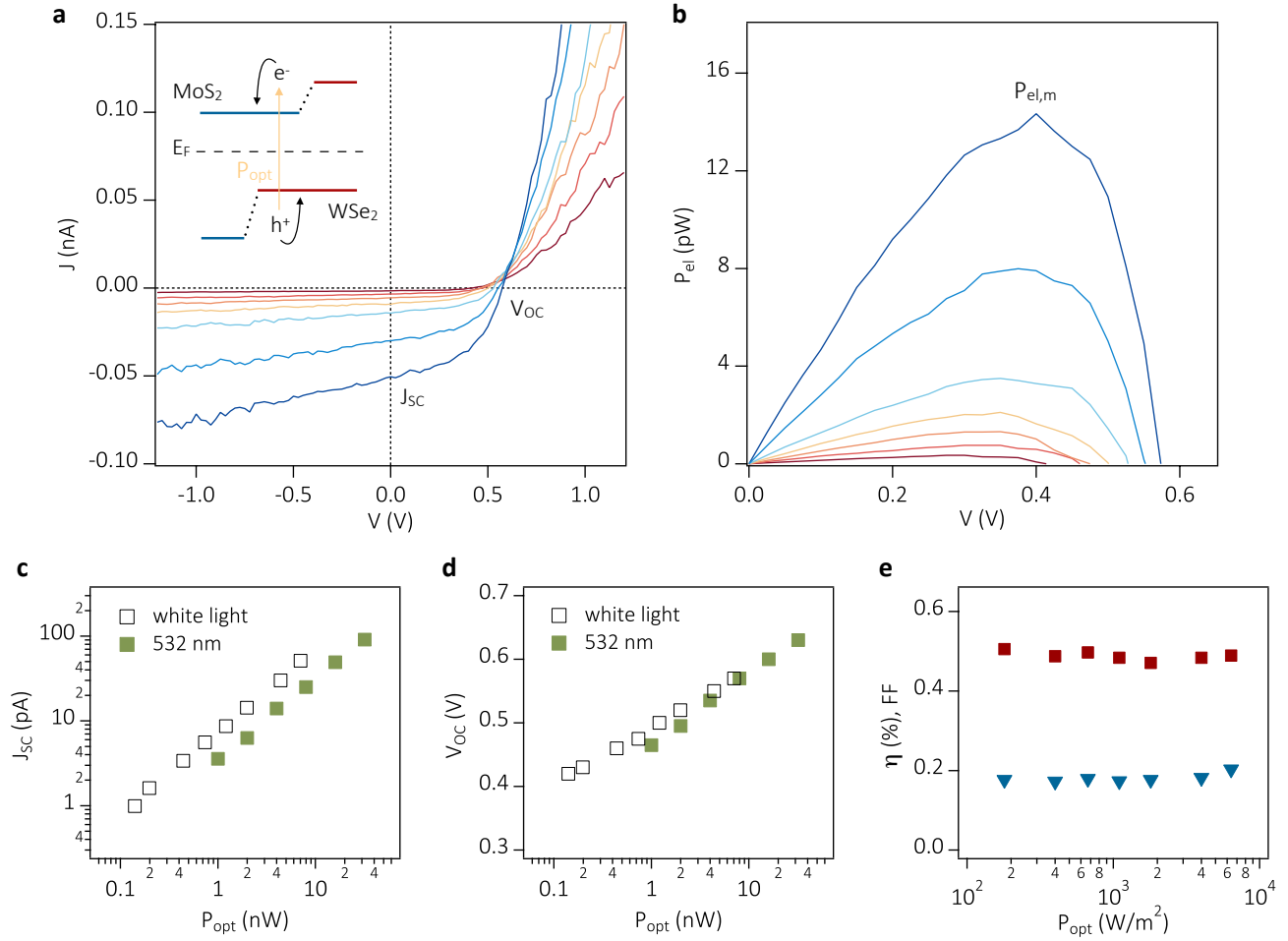


Figure 3. Photovoltaic properties of the heterojunction. (a) J - V characteristics of the device under optical illumination with $P_{\text{opt}} = 180, 400, 670, 1100, 1800, 4000,$ and 6400 W/m^2 . Inset: Schematic illustration of the photovoltaic effect: electron-hole pairs are generated in the heterostructure, relax to the bottom of the conduction and valence bands, and eventually diffuse to the contacts. (b) Electrical power, $P_{el} = J \cdot V$, that is extracted from the device. $P_{el,m}$ denotes the output in the maximum power point. (c) Short-circuit current J_{SC} and (d) open-circuit voltage V_{OC} , as extracted from Figure 3a (open symbols). The green symbols show results obtained from measurements with a 532-nm laser diode. (e) Fill factor FF (red rectangles) and power conversion efficiency η (blue triangles). During all measurements the gate bias was fixed at $V_G = -50 \text{ V}$.

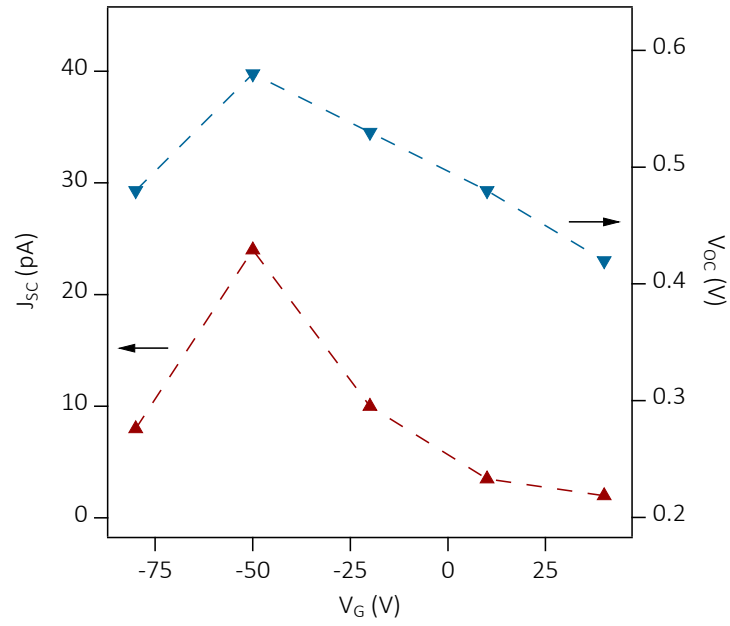
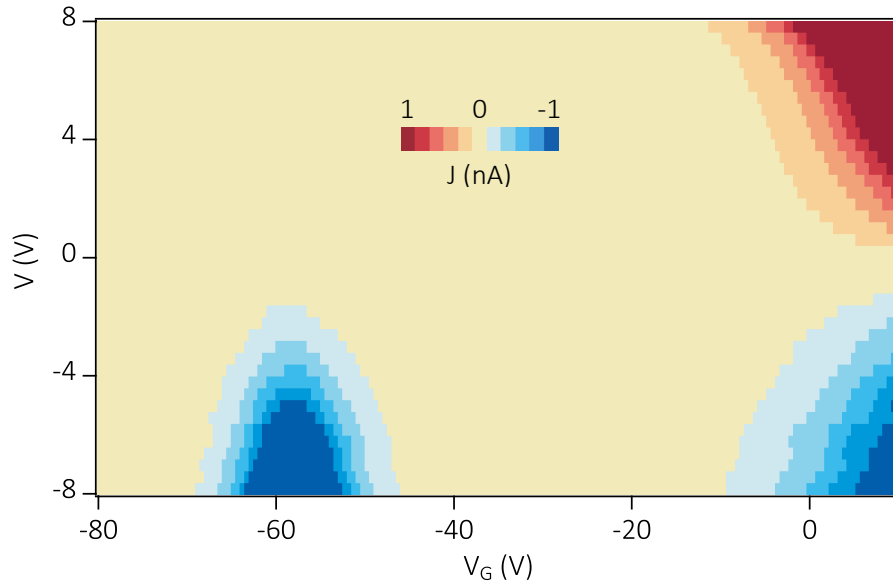


Figure 4. Gate voltage dependence of the photoresponse. Short-circuit current J_{SC} and the open-circuit voltage V_{OC} are shown as red and blue symbols, respectively ($P_{opt} = 3 \text{ kW/m}^2$).

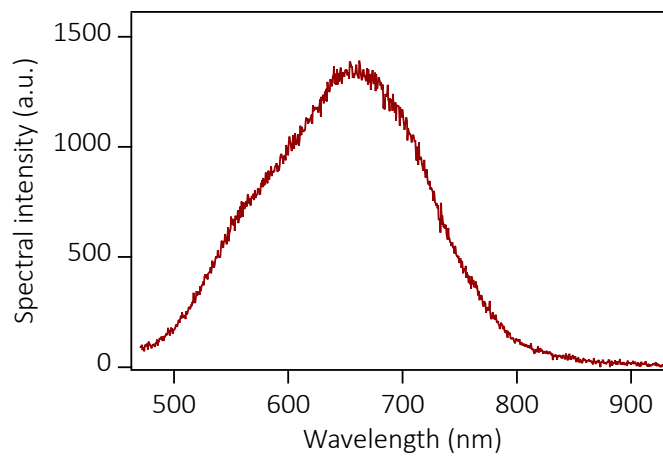
Supplementary Information

Photovoltaic effect in an electrically tunable van der Waals heterojunction

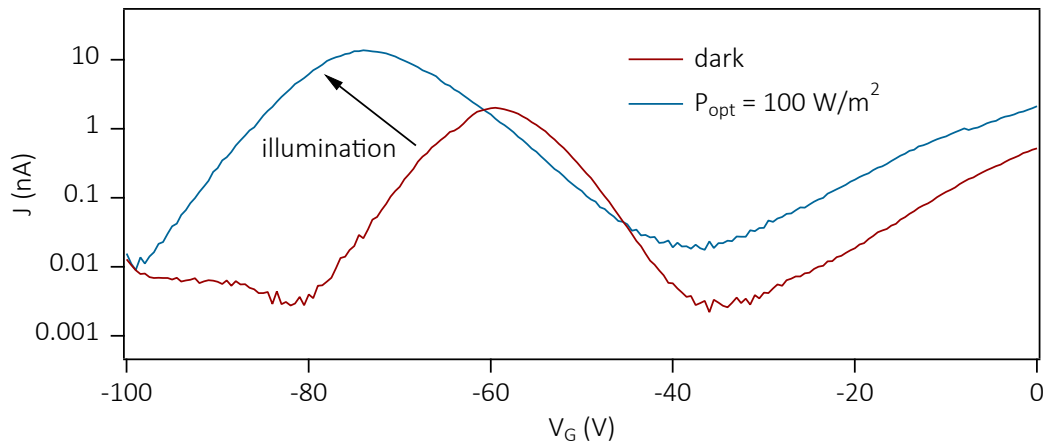
Marco M. Furchi, Andreas Pospischil, Florian Libisch, Joachim Burgdörfer, and Thomas Mueller



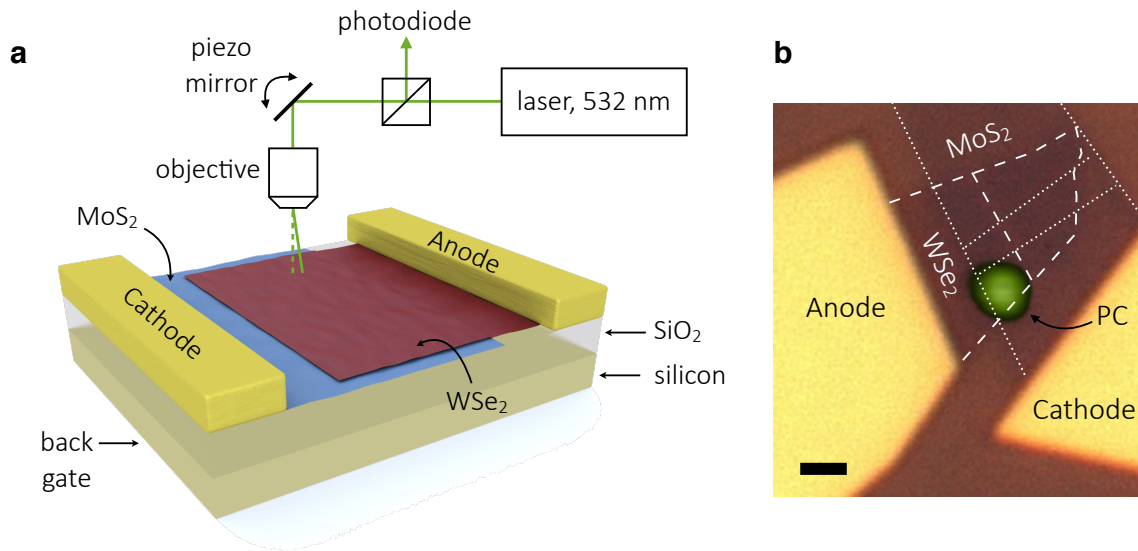
Supplementary Figure 1. Same measurement as in Figure 2a in the main paper, however, with different electrical wiring: MoS₂ sheet grounded; $-V$ applied to WSe₂. Voltage and current polarities are reversed, otherwise the device shows same behaviour: the WSe₂ sheet acts as anode and the MoS₂ as cathode.



Supplementary Figure 2. Emission spectrum of the halogen lamp.

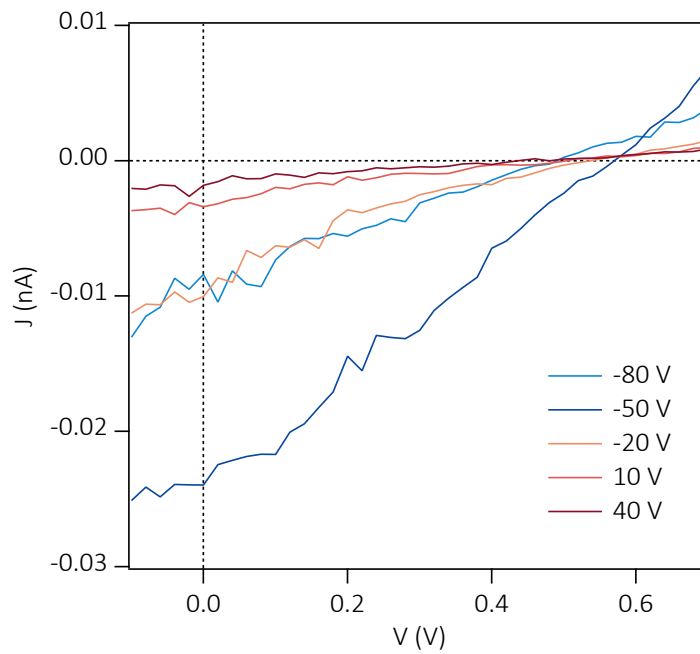


Supplementary Figure 3. Gate voltage dependence of device current recorded at $V = +8 \text{ V}$ plotted on a logarithmic scale. The red line is recorded in a dark probe station (same data as in Figure 2a in the main paper). Upon moderate illumination with 100 W/m^2 (blue line), the J - V_G broadens towards more negative gate voltages and the overall current increases by almost an order of magnitude. We recall that in our devices the “left-hand” off-state is attributed to depletion of the MoS_2 -sheet. The blue curve can thus be understood as a threshold voltage shift. A similar behaviour has previously been observed in conventional MoS_2 transistors³¹ and has been attributed to the photo-gating effect: optically excited carriers are captured in long-lived trap states and lower the barriers at the contacts, resulting in a larger current. Upon further increase of the incident optical power, the peak position remains rather stable and the forward current increases in accordance with Figure 3a in the main paper.



Supplementary Figure 4. (a) A solid-state laser (wavelength: 532 nm) was used as the excitation light source in the photocurrent imaging measurement. The laser beam was focused to a

diffraction-limited spot on the device using a microscope objective. A piezo-electrically driven mirror, mounted before the objective, scanned the beam across the sample. The edges of the contact electrodes were first located by detecting the reflected light from the sample with an external photodiode. The incident optical power was adjusted with neutral density filters. (b) Photocurrent image overlaid with an optical micrograph of the device. The MoS₂ and WSe₂ flakes are highlighted by dotted and dashed lines, respectively. The photocurrent (PC) is shown in green and stems from the overlap region between the two flakes. The flakes micro-crack due to handling, flexing, etc., during exfoliation and/or transfer (also shown as dashed and dotted lines), which currently restricts the area from which we can collect the photocurrent. Scale bar, 1 μm .



Supplementary Figure 5. J - V characteristics of the device under optical illumination with $P_{\text{opt}} = 3 \text{ kW/m}^2$ for gate voltages of -80, -50, -20, 10, and 40 V.